IEEE Photonics Journal
An IEEE Photonics Society Publication

Invited Paper

Time-Resolved Terahertz Spectroscopy of Free Carrier Nonlinear Dynamics in Semiconductors

Volume 2, Number 4, August 2010

G. Sharma
L. Razzari
F. H. Su
F. Blanchard
A. Ayesheshim
T. L. Cocker
L. V. Titova
H. C. Bandulet
T. Ozaki
J.-C. Kieffer
R. Morandotti
M. Reid
F. A. Hegmann

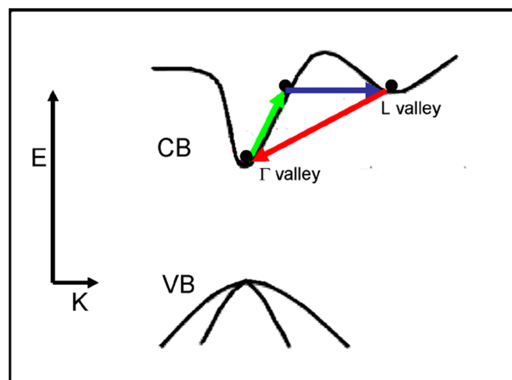

DOI: 10.1109/JPHOT.2010.2050873
1943-0655/$26.00 ©2010 IEEE

IEEE photonics SOCIETY
IEEE

Time-Resolved Terahertz Spectroscopy of Free Carrier Nonlinear Dynamics in Semiconductors

G. Sharma,[1] L. Razzari,[1,2] F. H. Su,[3] F. Blanchard,[1,4] A. Ayesheshim,[3] T. L. Cocker,[3] L. V. Titova,[3] H. C. Bandulet,[1] T. Ozaki,[1] J.-C. Kieffer,[1] R. Morandotti,[1] M. Reid,[5] and F. A. Hegmann[3]

(Invited Paper)

[1]INRS-EMT, Advanced Laser Light Source, Université du Québec, Varennes, QC J3X 1S2, Canada
[2]Dipartimento di Elettronica, Università di Pavia, 27100 Pavia, Italy
[3]Department of Physics, University of Alberta, Edmonton, AB T6G 2G7, Canada
[4]Graduate School of Science, Kyoto University, Kyoto 606-8502, Japan
[5]Department of Physics, University of Northern British Columbia, Prince George, BC V2N 4Z9, Canada

DOI: 10.1109/JPHOT.2010.2050873
1943-0655/$26.00 ©2010 IEEE

Manuscript received April 20, 2010; accepted May 14, 2010. Date of publication May 20, 2010; date of current version June 18, 2010. This work was supported by the Natural Sciences and Engineering Research Council of Canada (NSERC), NSERC Strategic Projects, le Fonds Québécois de la Recherche sur la Nature et les Technologies (FQRNT), and the INRS. L. Razzari was supported by a Marie Curie Outgoing International Fellowship under Contract 040514. Corresponding author: L. Razzari (e-mail: luca.razzari@emt.inrs.ca).

Abstract: Nonlinear dynamics of free carriers in direct bandgap semiconductors at terahertz (THz) frequencies is studied using the intense few-cycle source available at the Advanced Laser Light Source (ALLS). Techniques such as Z-scan and optical-pump/THz-probe are employed to explore nonlinear interactions in an n-doped InGaAs thin film and a photoexcited GaAs sample, respectively. The physical mechanism that gives rise to such interactions is found to be intervalley scattering. A simple Drude-based mathematical model that incorporates the intervalley scattering process is developed and agrees well with the THz response of free carriers in semiconductors.

Index Terms: Intervalley scattering, semiconductors, terahertz pulses, time-resolved terahertz spectroscopy, ultrafast nonlinear optics, z-scan.

1. Introduction

Ultrafast terahertz (THz) optics has developed at a remarkably fast rate over the last two decades, driven in part by its wide scope of applications in spectroscopy of physical, chemical, and biological samples [1]–[5]. However, THz nonlinear optics has been relatively unexplored, due to the lack of high-energy, few-cycle THz sources. Up to now, there have been several studies using nanosecond to microsecond duration intense THz pulse sources with incoherent detection methods [6]–[10]. For example, there have been reports of third harmonic generation in bulk semiconductors using far infrared sources [7], while a nonlinear response associated to quantum confined electrons in nonparabolic subbands has been observed in semiconductor nanostructures [8]. Further, impact ionization in InAs heterostructures, as well as a change in the absorption peak of multiple quantum wells under the influence of a strong THz electric field, have been recently reported [9], [10]. The

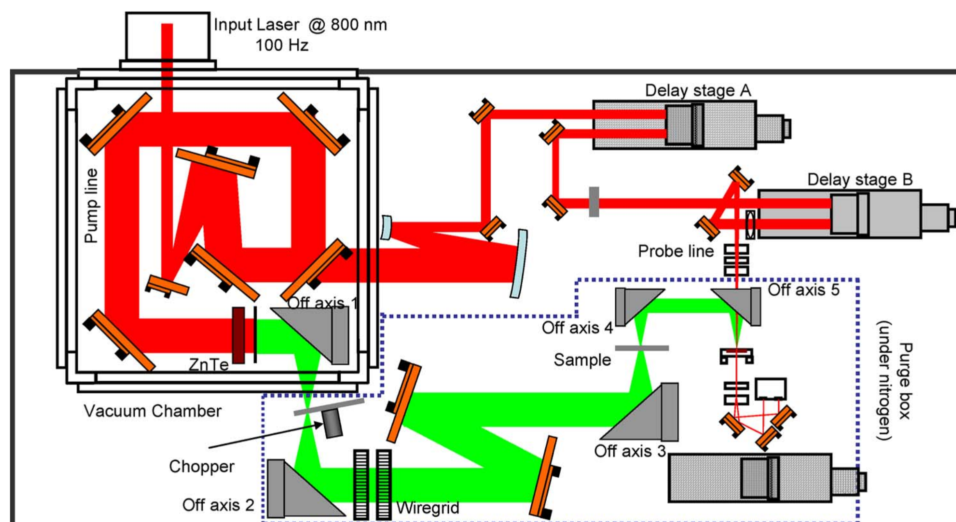

Fig. 1. Schematic of the high-intensity THz pulse source at the Advanced Laser Light Source (ALLS) (adapted from [15]).

ultrafast pulse slicer technique has also been used to study Rabi oscillation in the population of two low-lying states of donor impurities of GaAs over a picosecond timescale [11].

With the recent development in laser-based intense, few-cycle THz sources, and coherent detection techniques [12]–[18], it is now possible to study the nonlinear optical response of materials at THz frequencies and at picosecond (and even sub-picosecond) timescales. For example, a long-lived coherent THz emission centered around 2 THz and carrier-wave Rabi oscillations have been observed between bound impurity levels of n-type GaAs, excited by an intense THz pulse with electric field amplitude of 70 kV/cm [12], [19]. In addition, THz-intensity-dependent cross-phase modulation (XPM) has been observed in electrooptic (EO) crystals, in turn leading to spectral shifting, broadening, and modulation of co-propagating laser pulses [13], [20]. Lattice anharmonicity and self-phase modulation (SPM) in $LiNbO_3$ [17] and THz-electric–field-induced impact ionization in InSb [21], [22] have been reported using intense THz pulses. Moreover, these sources have allowed the observation of a decrease in THz absorption due to intervalley scattering in doped GaAs, Si, and Ge using THz-pump/ THz-probe techniques [23], [24], and recently, they have also enabled the detection of the Kerr effect at THz frequencies, in which a THz intensity dependent birefringence is induced in liquids [25].

In this paper, we will review the nonlinear THz experiments performed using the intense THz source available at the Advanced Laser Light Source (ALLS) in Canada [15]. In particular, we will describe i) the nonlinear absorption bleaching of intense THz pulses in an n-doped InGaAs thin film, due to THz-electric-field-driven intervalley scattering of electrons in the conduction band. This effect was observed by using an open aperture Z-scan technique [26]. In addition, we will report on ii) the nonlinear transient absorption bleaching in photoexcited GaAs using an optical-pump/THz-probe (OPTP) technique [27].

This paper is organized as follows. In Section 2, we will describe the large aperture zinc telluride (ZnTe) THz source, which has been used to perform the nonlinear THz experiments described here. In Section 3, we will discuss in detail the experimental observations of the absorption bleaching in n-doped InGaAs films revealed by our Z-scan technique. This will be followed by a discussion on the theoretical background of THz absorption bleaching in semiconductors and by comparing the experimental results with the developed model. Finally, in Section 4, we will report the results of our experiments on photoexcited GaAs using the OPTP technique.

2. THz Source

In our experiments, high-energy THz pulses are generated by optical rectification in a large aperture (75-mm diameter) ZnTe single crystal wafer [15], [28]. The Ti:sapphire laser beam lines of the ALLS used in these experiments operates at a repetition rate of 100 Hz and provides 800-nm, $\sim$40-fs laser

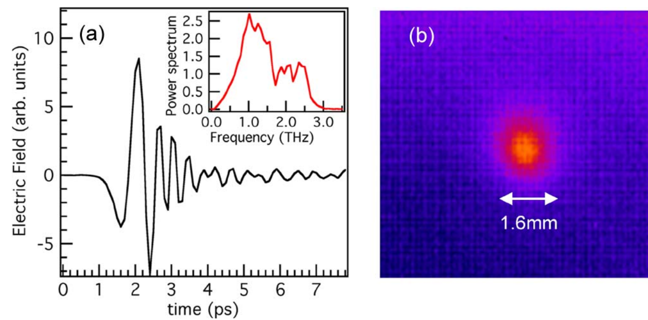

Fig. 2. (a) Electric field profile of the terahertz beam emitted by the ZnTe optical rectification source. The inset shows the power spectrum of the THz pulse. (b) Pyroelectric detector array image of the THz spot-size at the focus with a $1/e^2$ diameter of 1.6 mm (adapted from [26]).

pulses with energies as high as 48 mJ per pulse (at the ZnTe crystal position). The experimental setup, shown in Fig. 1, comprises three main parts: i) a THz generation chamber held under vacuum ($< 10^{-6}$ Torr), ii) an 800-nm probe line in air, and iii) a dry-nitrogen-purged THz propagation line. The THz emitter consists of a 1-mm-thick (110) ZnTe single crystal wafer with a diameter of 75 mm. To minimize saturation and to avoid damage to the crystal surface, the 800 nm beam is spatially expanded to about 36 cm^2 (area calculated at $1/e^2$ of the maximum) at the surface of the ZnTe emitter. Any remaining 800 nm light transmitted through the ZnTe wafer is blocked using a black polyethylene absorber, which is transparent to THz radiation. Five off-axis parabolic mirrors are used after the THz generating crystal to redirect the THz wave to the detector, with three focus positions: i) at the exit of the vacuum chamber, ii) at the sample position for spectroscopy, and iii) at the ZnTe detector crystal for EO sampling. A chopper positioned at the first focus allows modulation of the THz beam for lock-in detection. Two 4-in diameter wire-grid polarizers (Microtech Instruments model G30L) are used to control the intensity and the polarization of the THz beam.

To detect the THz pulse waveform, we use free-space EO sampling in a second, 0.5 mm thick, (110) ZnTe crystal [29], [30]. A lock-in amplifier connected to the output of a pair of photodiodes and referenced to the chopper is used to acquire the THz waveforms.

The source provides picosecond THz pulses in the frequency range of 0.1–3 THz with μJ-level energies. Fig. 2(a) shows an example of the temporal profile of the THz pulse produced by our source, and the inset shows the corresponding power spectrum. These pulses are focused by an off-axis parabolic mirror down to a spot size of 1.6 mm (full-width at $1/e^2$ maximum) at the second focal position (i.e., the sample position). We used a $BaSrTiO_3$ (BST) pyroelectric infrared camera (Electrophysics model PV320-L2V) to image the THz spot at the focus. This camera operates with an internal 10 Hz chopper and has a 320×240 pixel imaging array with a pixel spacing of 48.5 μm. Fig. 2(b) shows the THz image obtained using 0.8 μJ THz pulses. The THz beam profile is found to be well fitted by a Gaussian shape. To measure the THz energy, we used a calibrated pyroelectric energy detector (Coherent Molectron J4–05) [15].

3. Z-Scan Measurements

Using the experimental set-up presented in Section 2, we performed an open aperture Z-scan measurement [31]. Z-scan is a very common and straightforward nonlinear characterization technique used to determine intensity dependent transmission change in a given sample. When performing a Z-scan measurement, the transmittance of the sample is measured as the sample is moved along the propagation path z of a focused THz beam, as depicted in Fig. 3. Whenever nonlinear absorption takes place, the intensity of the transmitted THz beam depends on the spot size of the beam at the sample position. Clearly, THz intensity is maximum at the focus and is progressively reduced as the sample is moved away from the focus (in both directions). This method is widely used in multiphoton absorption studies [32], [33] and has proven to be effective, even for the characterization of saturable absorbers [34].

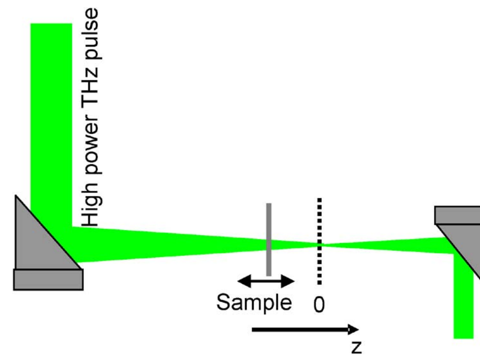

Fig. 3. Schematic of Z-scan. THz beam is focused using an off axis mirror and the sample is placed close to the focus and translated along the propagation direction of the THz beam, across the focal position.

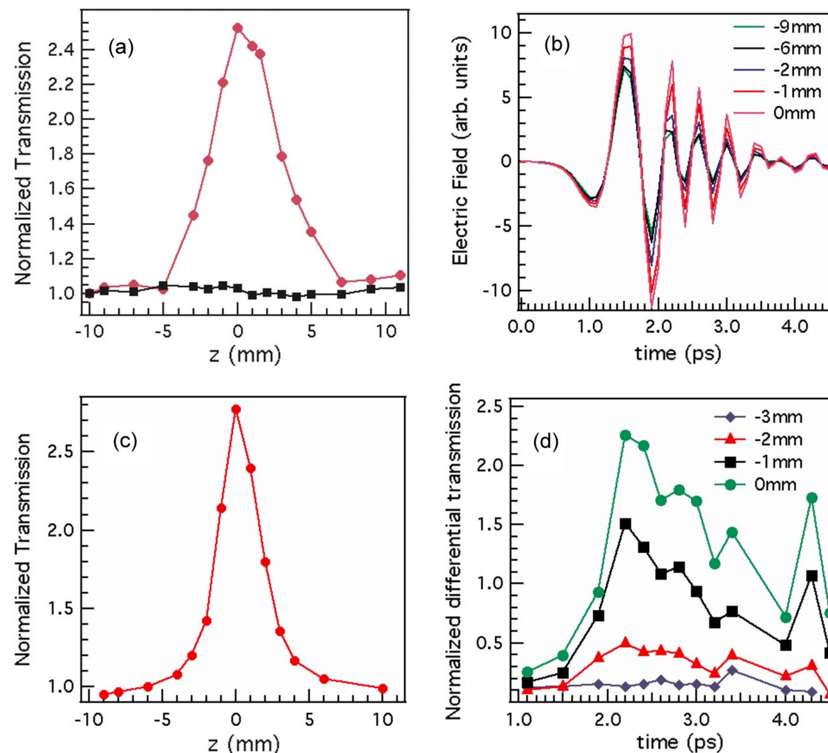

Fig. 4. (a) Z-scan normalized transmission of the total THz pulse energy measured with a pyroelectric detector after the sample (the purple curve refers to the InGaAs epilayer on an InP substrate and the black curve to the InP substrate only). (b) Transmitted THz pulse electric field for different positions of the Z-scan. (c) Normalized time integral associated with the modulus squared of the transmitted electric field as a function of the z position along the scan. (d) Normalized electric field differential transmission as a function of time for different z positions along the scan (adapted from [26]).

The sample we used for this experiment was a thin film of a heavily doped direct bandgap semiconductor, namely Indium Gallium Arsenide. Specifically, it consists of a 500-nm-thick n-type $In_{0.53}Ga_{0.47}$ As epilayer with a doping concentration of about 2×10^{18} cm^{-3} grown by metal-oxide chemical vapor deposition on a lattice-matched, 0.5 mm-thick semi-insulating InP substrate. At low excitation levels, the sample transmits about 3% of the incident THz energy. We have confirmed that this strong THz absorption is mainly due to the high conductivity of the epilayer, since measurements of the InP substrate alone have shown an overall THz transmission (including absorption and reflection losses) of about 60%.

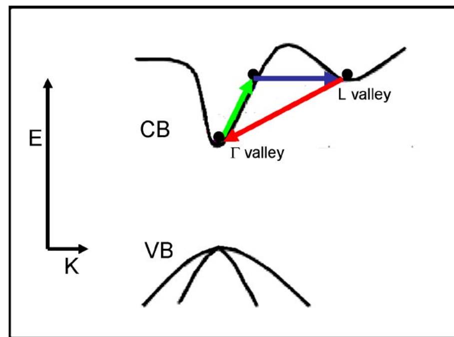

Fig. 5. Mechanism of intense THz pulse induced intervalley scattering. The electrons in the conduction band are accelerated by the THz electric field (green arrow); after acquiring enough kinetic energy, they may scatter into a satellite valley (L valley in this case, blue arrow) from which they then have a finite probability to scatter back to the bottom of the conduction band (red arrow).

In order to explore the nonlinearity of the sample, we first used a previously calibrated pyroelectric detector, which measures directly the THz energy. We measured the total transmitted THz pulse energy as a function of the z position of the sample. As shown in Fig. 4(a), when the sample is illuminated by 0.8-μJ THz pulses (with a peak electric field of about 200 kV/cm), we observe a significant enhancement in the transmission near the focus, in contrast to the transmission away from the focus. Fig. 4(a) also shows that this dramatic absorption bleaching effect is not observed when the same scan is performed on a bare InP substrate.

Next, we measured the temporal profile of the transmitted THz electric field at different z-positions. Fig. 4(b) shows no significant temporal shift between the transmitted pulses, so we can conclude that the imaginary part of the conductivity is not appreciably changing in our measurement. One can also see that the transmission enhancement changes with time, with dynamical features on a timescale comparable with the THz pulse duration. By taking the time integral of the modulus squared of these traces, one obtains a quantity proportional to the transmitted energy [see Fig. 4(c)], which is found to be consistent with the direct energy measurement shown in Fig. 4(a).

The dynamics of the bleaching process is more evident in Fig. 4(d), where we plot the normalized electric field differential transmission (defined as the transmitted electric field difference between the actual position in the Z-scan and a position far away from the focus, for each peak of the THz pulse) as a function of time for different z positions along the scan. The curves show an initial increase in transmission over a period of 1 ps (with a peak at $t = 2.2$ ps) followed by a slower decay.

It is important to note that a frequency-domain analysis of the process yields misleading results. This is because the chirp in the THz pulse waveform, which is always present in ultrashort THz pulses, creates artificial frequency dependencies of the bleaching process, since different temporal sections of the waveform (and therefore different frequency components) have different amplitudes. Thus, it is necessary to study nonlinear THz pulse interactions in the time domain. We developed and used a time-dependent model to understand this observation, as discussed in the next section.

3.1. Theoretical Background

In the above measurement, we have found evidence of absorption bleaching of intense THz pulses in n-doped InGaAs. The absorption bleaching observed during the interaction of intense THz pulses with the electrons in the conduction band of the InGaAs sample can be attributed to THz-induced intervalley scattering between non-equivalent valleys. In particular, we have focused our attention on the electron dynamics in the Γ and the L valley (which is the closest upper valley in InGaAs) of the conduction band of the sample under investigation. Absorption bleaching of intense THz pulses can be explained as follows. Free carriers in the Γ valley are accelerated by the THz electric field during each oscillation. When the carriers acquire enough kinetic energy to overcome the nearest intervalley

separation, they may scatter into an upper valley (i.e., the L valley), as shown in Fig. 5. Since the effective mass of electrons is higher in the L valley, the carrier mobility is lower, thus reducing the overall conductivity of the semiconductor film. Since the transmission of the THz pulse increases with a decrease in the conductivity of the sample, the transmission is enhanced at high THz electric fields, when carriers are scattered to the upper satellite valley. The electrons in this upper valley will then have a finite probability of scattering back to the Γ valley, where the effective mass is smaller. Therefore, the conductivity of the film will eventually increase back to its original value, which will eventually result in a decrease in the THz transmission.

3.2. Dynamic Intervalley-Electron-Transfer Model

A simple Drude-based model incorporating Γ–L intervalley scattering is used to describe the temporal dynamics of the observed nonlinear THz transmission. The THz transmission of our sample, which can be idealized as a thin conducting sheet with thickness d on an insulating substrate with index N, can be expressed as follows [35]:

$$E_{\text{trans}}(t) = \frac{1}{Y_0 + Y_s}(2Y_0 E_{\text{inc}}(t) - Jd). \tag{1}$$

Here, E_{trans} and E_{inc} are the transmitted and incident THz fields, $Y_0 = (377\Omega)^{-1}$ and $Y_s = NY_0$ are the free-space and substrate admittances, respectively, and J is the current density in the film, which is given by

$$J = n_\Gamma \nu_\Gamma e + n_L \nu_L e \tag{2}$$

where e is the electronic charge, n_Γ and n_L are the electron densities, and ν_Γ and ν_L are the drift velocities of the Γ and L valley. The electron velocities driven by the transmitted THz field E_{trans} and the population of electrons in the Γ valley n_Γ can be described by the dynamic equations

$$\frac{dv_i}{dt} = \frac{eE_{\text{trans}}}{m_i^*} - \frac{v_i}{\tau_i} \qquad i = \Gamma, L \tag{3}$$

$$\frac{dn_\Gamma}{dt} = -\frac{n_\Gamma}{\tau_{\Gamma L}} + \frac{n_L}{\tau_{L\Gamma}} \tag{4}$$

$$n_0 = n_L + n_\Gamma. \tag{5}$$

Here, τ_Γ, τ_L and m_Γ^*, m_L^* denote the intravalley scattering times and the effective masses in the two valleys, while $\tau_{L\Gamma}^{-1}$ and $\tau_{\Gamma L}^{-1}$ are the scattering rates from one valley to the other, and n_0 is the total electron density. During the absorption bleaching process, the transmitted field E_{trans} accelerates the electrons in the conducting layer of the sample and induce the population transfer between the different valleys of the conduction band. This in turn affects the current density J in (1), and hence modifies the transmitted field. This feedback is responsible for the rich and surprising dynamical features associated with the effect under investigation. The change in the electron population of the Γ and L valleys is determined by the intervalley scattering rates. The L–Γ transfer rate $\tau_{L\Gamma}^{-1}$ is kept constant [36], while the Γ–L scattering rate $\tau_{\Gamma L}^{-1}$ is a function of the average kinetic energy of the electrons in the Γ valley [37]:

$$\varepsilon_\Gamma = \frac{1}{2} m_\Gamma^* v_\Gamma^2 + \frac{3}{2} k_B T_L. \tag{6}$$

This average kinetic energy is associated with the electrons in the Γ valley. The scattering rate $\tau_{\Gamma L}^{-1}$ is zero at low energies but starts to increase rapidly at a threshold value ε_{th} to a maximum value $\tau_{\Gamma L0}^{-1}$ at high energies

$$\tau_{\Gamma L}^{-1}(\varepsilon_\Gamma) = \begin{cases} 0, & \varepsilon_\Gamma \leq \varepsilon_{\text{th}}(1-b) = \varepsilon_1 \\ \text{smooth function for} & \varepsilon_1 < \varepsilon_\Gamma < \varepsilon_2 \\ \tau_{\Gamma L0}^{-1}, & \varepsilon_\Gamma \geq \varepsilon_{\text{th}}(1+b) = \varepsilon_2. \end{cases} \tag{7}$$

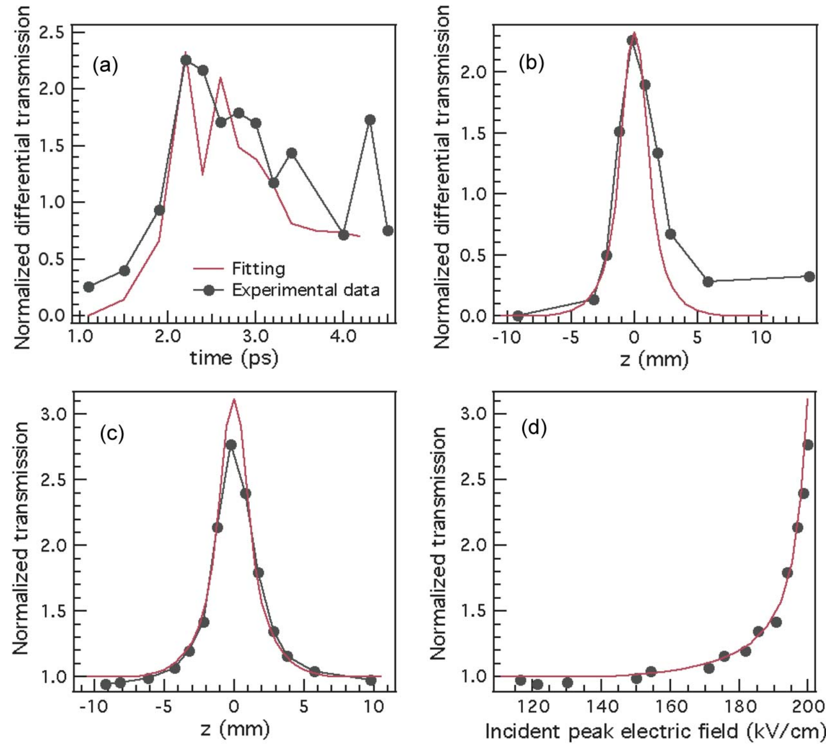

Fig. 6. (a) Normalized electric field differential transmission as a function of time at the focus of the Z-scan (purple line: model; gray line: experimental data). (b) Peak value ($t = 2.2$ ps) of the normalized electric field differential transmission as a function of the z position along the scan. (c) Comparison with the data from Fig. 5(c). (d) Incident electric field dependence of the normalized energy transmission (adapted from [26]).

Since intervalley scattering takes place via the emission or absorption of optical phonons, the energy-dependent function of the valley transfer rate, $\tau_{\Gamma L}^{-1}(\varepsilon_\Gamma)$, is tentatively made "smooth." The smooth function is inserted via a seventh-order polynomial section that is continuous up to the third derivative [37]. Here, ε_{th} and b are the threshold energy and smooth width parameter, respectively. Nonparabolic effects are considered by assuming that the effective masses for Γ and L valley varies as

$$m_\Gamma^*(\varepsilon_\Gamma) = m_{\Gamma 0}^*(1 + \alpha_\Gamma \varepsilon_\Gamma) \tag{8}$$

$$m_L^*(\varepsilon_L) = m_{L0}^*(1 + \alpha_L \varepsilon_L). \tag{9}$$

Here, α_Γ and α_L are the nonparabolicity parameters for the Γ and L valley in the sample, and $m_{\Gamma 0}^*$ and m_{L0}^* are the effective masses at the valley minima.

We find that this simple model is adequate to explain the obtained results, as described below. Electric-field-driven intervalley scattering is a well-known mechanism in high-field transport physics, and it can introduce negative differential resistance and Gunn oscillations in direct bandgap semiconductors [38]. The critical DC field required to excite these phenomena in $In_{0.53}Ga_{0.47}As$ is usually in the range of 2.5–4 kV/cm [39]. However, at THz frequencies, the critical field required to excite the same phenomenon can be higher than its DC counterpart. We have observed in our measurement that the effect of absorption bleaching vanishes rapidly, as the peak electric field inside the epilayer drops below 14 kV/cm (at position $z = \pm 4$ mm in the Z-scan).

Fig. 6 shows how the model presented above can describe both the transmitted energy and the time-domain experimental results, strongly suggesting that the intervalley scattering mechanism is responsible for the observed nonlinear process. Table 1 summarizes the parameters used in the

TABLE 1

Model parameters for n-doped InGaAs

Parameters	Symbols	Simulation parameters	References
Effective mass ratio	$m^*_{\Gamma 0}$	Γ valley:0.03745	[40]
	m^*_{L0}	L valley: 0.26	[40]
Nonparabolicity factor (eV^{-1})	α_Γ	Γ valley: 1.33	[40]
	α_L	L valley: 0.59	[40]
Refractive index of InP	N	3.1	[41]
Threshold energy (eV)	ε_{th}	0.13	0.25 [43] (a)
Smooth parameter	b	0.57	
Intravalley scattering rate (s^{-1})	τ_Γ^{-1}	Γ valley: 1.0 x10^{13}	
	τ_L^{-1}	L valley: 1.67x10^{13}	
Γ-L intervalley scattering rate (s^{-1})	$\tau_{\Gamma L0}^{-1}$	3.33 x10^{13}	2.50x10^{13} [42] (b)
L-Γ intervalley scattering rate (s^{-1})	$\tau_{\Gamma L}^{-1}$	2.50 x10^{11}	3.23x10^{11} [41]

a) We estimated that the threshold energy is lower than 0.25 eV according to the Monte Carlo calculation reported on doped $In_{0.53}Ga_{0.47}As$ in Ref. [43].
b) The Γ-L intervalley scattering rate of GaAs reported in Ref. [42] is about 2.50 x 10^{13} s^{-1}.

simulation [40]–[42]. As one can see, the threshold energy value ε_{th} for the scattering rate that one has to assume in order to fit the experimental data (0.13 eV) is lower than the intervalley separation commonly found in literature (0.55 eV). This is most probably because our simplistic model does not consider the electron temperature, which is usually a significant term in the electron energy equation. However, the ability of our model to properly describe the dynamics of the process is demonstrated by the maximum drift velocity predicted at the focal position, which is around 9×10^7 cm/s. Calculations made by other groups have shown that this value, which is limited by intervalley scattering in n-doped InGaAs, can reach 10^8 cm/s at a time of 200 fs after applying an electric field of 20 kV/cm [43]. Since the effective mass of the electron in InGaAs is about 0.04 m_e, this maximum velocity overshoot value corresponds to a kinetic energy of about 0.11 eV, which is much less than the Γ–L energy separation of 0.55 eV but close to the threshold energy of 0.13 eV obtained from our data fitting. The fitting procedure allows one to quantify the scattering rates of heavily doped InGaAs, as studied here. The Γ–L intervalley scattering rate is found to be about 3.33×10^{13} s^{-1}, close to the value measured in GaAs [42], while the L-Γ intervalley relaxation rate is found to be about 2.50×10^{11} s^{-1}, which is similar to that found in [34]. Using this model we can also describe the rapid transmission change along the Z-scan [see Fig. 6(c)].

The process is highly nonlinear, as seen in Fig. 6(d), where the normalized transmission is plotted as a function of the estimated incident field strengths along the Z-scan. It should be noted that this nonlinear behavior cannot be reproduced by any two-level system saturation model, such as the one reported in [32], and it offers further evidence of the intervalley bleaching mechanism discussed here. In particular, it is also worth stressing that THz Z-scan gives access to the dynamics of a nonlinear process by simply measuring the change in transmission of a single THz pulse, which is something that is usually not possible at optical frequencies.

Up to now, there has been only one other THz Z-scan experiment performed, using an undoped InSb sample [21]. In this paper, absorption enhancement due to impact ionization effects has been reported, which is the contrary to what has been observed in our measurements, where absorption bleaching due to intervalley scattering has been observed. Nonlinear bleaching of THz pulse absorption was reported in n-doped Ge and GaAs in a pioneering work [7], by using 40-ns THz pulses. This phenomenon was attributed to a THz-electric-field-induced scattering of carriers into satellite valleys of the conduction band. However, since the THz pulse had nanosecond duration

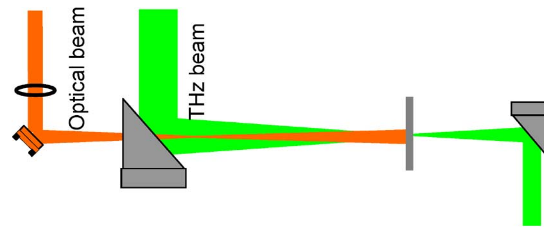

Fig. 7. Schematic of the optical-pump-THz-probe technique. The sample is placed at the focus of the THz beam, between two off axis mirrors. An optical beam is sent through a hole in the off axis and illuminates the sample.

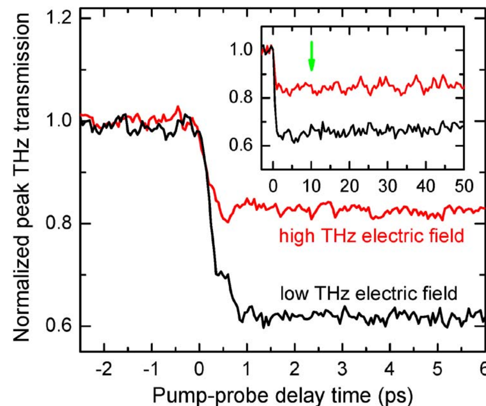

Fig. 8. Normalized transmission of the peak electric field of a THz pulse at low and high THz fields as a function of the delay time with respect to a 800-nm, 40-fs, optical pump pulse. The inset shows the corresponding long-term dynamics and the delay at which the waveforms shown in Fig. 9 were taken (green arrow at 10 ps) [27].

[7], it was not possible to resolve the ultrafast dynamics of the nonlinear mechanism. Through the experiments described above, owing to the intense few-cycle THz pulses at our disposal and the coherent detection technique based on EO sampling, we believe we have unveiled the ultrafast nature and the real dynamics of this phenomenon.

4. OPTP Experiment

We have also used an optical-pump/intense THz-probe (OPTP) technique to explore the nonlinear electron dynamics of undoped GaAs [27]. The OPTP experiment is performed on a 0.5-mm-thick semi-insulating (SI)-GaAs wafer. Again, we use the intense THz source described in Section 2 for this experiment. The sample is placed at the focus of the THz beam, and an optical pump beam (800 nm wavelength, 40 fs pulse duration, 8 $\mu J/cm^2$ fluence) is used to photoexcite the sample, as shown in Fig. 7.

At the sample position, the spot size of the THz probe beam and the optical pump beam are 1.6 mm and 12 mm, respectively. Before detection, in the arm where the THz beam is collimated, we placed two wire grid polarizers to keep the THz electric field within the linear detection regime of the detector crystal. We further used other wire-grid polarizers and Si wafers to adjust the amplitude of the THz probe pulse at the sample position. All experiments were performed under a dry nitrogen purge at room temperature.

First, we measured the THz transmission, sitting on the peak of the THz pulse, as a function of the pump-probe delay time. This is a common method for probing ultrafast carrier dynamics in semiconductors in linear OPTP [44], [45]. We have studied high and low THz-probe field transmission in photoexcited GaAs, where high and low fields correspond to 173 kV/cm and 4 kV/cm,

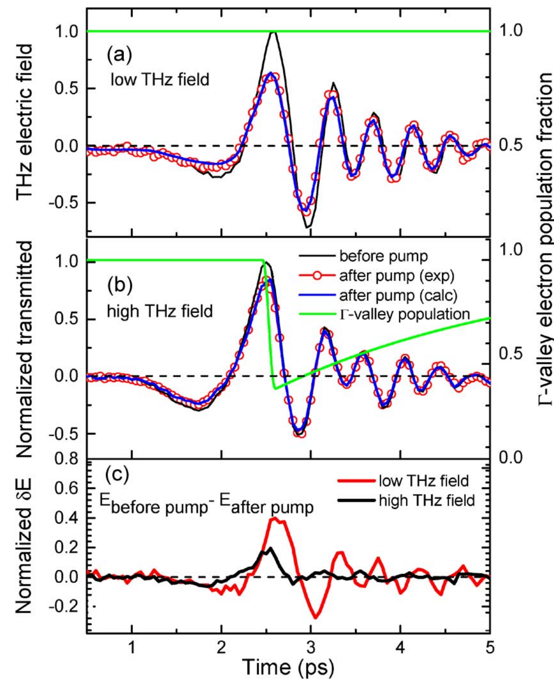

Fig. 9. Transmitted THz waveforms measured 10 ps before and after photoexcitation. (a) Low and (b) high THz probe fields. The blue lines represent the best fit obtained using the dynamic intervalley-electron-transfer model. The green line shows the fraction of electrons in the Γ valley according to model calculations (adapted from [27]). (c) Experimental THz electric field difference (δE), as obtained from (a) and (b).

respectively. Fig. 8 shows the THz transmission as a function of pump-probe delay time for high and low THz fields, respectively. The inset shows the long-term dynamics.

The 800-nm pump pulse photoexcites electron-hole pairs in the normally insulating GaAs sample. Since holes in GaAs have a significantly lower mobility when compared to electrons, we can safely neglect the contribution of the holes to the overall conductivity of the sample. Photoexcited electrons are then injected into the higher mobility central Γ valley in the conduction band. At low THz probe fields, the transmission of the THz pulse through the photoexcited GaAs sample is approximately 60% of the transmission through the unexcited sample. However, at high THz probe fields, the relative change in transmission is greatly reduced, in comparison with the low THz probe field, suggesting that THz absorption bleaching is again taking place. As in the case of doped InGaAs, we suppose that the absorption bleaching observed at high THz probe fields in photoexcited GaAs is due to THz-pulse-induced intervalley scattering of electrons between the Γ and L valleys of the conduction band [46]–[48]. It is well known that optically induced intervalley scattering in ultrafast pump-probe and OPTP experiments (performed using higher pump photon energies, e.g., 400-nm pump pulses) can excite carriers directly into the satellite valleys via optical phonon scattering [34], [35], [45], [49]–[51]. In addition, the observation of electric-field-induced intervalley scattering has recently been reported in OPTP experiments in DC-biased GaAs wafers [52]. However, here we show intervalley scattering induced by the THz probe pulse itself in an OPTP experiment.

Fig. 9 shows the transmitted THz waveforms measured at a pump-probe delay time of 10 ps. These waveforms were normalized to the peak of the THz waveform transmitted through the unexcited sample at negative delay times. Absorption bleaching can be clearly seen in the relative amplitude of the transmitted THz waveform at high THz fields, compared with that at low THz fields. In particular, there is almost no change in electric-field amplitude or phase shift in the trailing portion of the THz waveform at high THz probe fields. We note that the observed absorption bleaching is inconsistent with an impact ionization mechanism, as impact ionization would induce an

TABLE 2

Model parameters for GaAs

Parameters	Symbols	Simulation parameters
Carrier Concentration (cm^{-3})	n_0	1.7 x10^{17} [27]
Intravalley scattering rate (ps)	τ_Γ	0.16 Low Field [27] 0.051 High Field [27]
Threshold energy (eV)	ε_{th}	0.16 [27]
Γ-L intervalley scattering rate (ps)	$\tau_{\Gamma L0}$	0.022 [27]
L-Γ intervalley scattering rate (ps)	$\tau_{L\Gamma}$	3.0 [27]

enhancement in THz pulse absorption [21], [22]. In Fig. 9(c), we present the transmitted THz electric field difference (δE) before and after the optical pump, under low and high THz probe fields, respectively. Since the optical penetration depth at 800 nm is around 1 μm for GaAs, we can safely use (1) once again to describe the THz transmission through the sample. As it can be easily shown, δE is thus proportional to the current J, as well as to the average drift carrier velocity driven by the THz electric field. Fig. 9(c) shows that the high-field THz induced current/carrier average velocity, exhibits remarkable saturation effects, when compared with the low-field THz probe case. In particular, there is an abrupt drop of the absolute value of δE along the trailing edge of the THz pulse (after $t = 2.8$ ps in Fig. 9). This indicates that the carrier velocity becomes strongly nonlinear, when the optically excited GaAs is probed by a high-field THz pulse.

Once again, we can use the model developed in Section 3 for a thin conductive layer experiencing THz induced intervalley scattering. From the fitting of the low-field data [see Fig. 9(a)], the total carrier density and the intravalley relaxation time can be obtained, resulting in a value $n_0 = 1.7 \times 10^{17}$ cm^{-3} and $\tau_\Gamma = 0.16$ ps, respectively. This corresponds to a carrier mobility of 4200 cm^2/Vs, which is consistent with other OPTP experiments in GaAs [45]. This is also consistent with a total carrier density of about 1.9×10^{17} cm^{-3}, estimated from the measured pump fluence incident on the sample and assuming a pump beam reflectance of about 40%. At high THz fields, the same value for n_0 is used as in the low-field case. The best fit to the observed THz transmission [Fig. 9(b)] gives $\tau_\Gamma = 0.051$ ps and requires intervalley scattering with $\tau_{\Gamma L0} = 0.022$ ps and $\tau_{L\Gamma} = 3.0 \pm 1.0$ ps. The initial Γ–L population transfer occurs over a timescale of 77 fs, which is comparable to the Γ–L intervalley scattering time of about 80 fs reported elsewhere [42]. The transfer time back to the Γ valley of $\tau_{L\Gamma} = 3.0 \pm 1.0$ ps also agrees well with the approximately 2 ps transfer times reported in other OPTP experiments [49], [51]. The threshold energy extracted from the fitting is $\varepsilon_{th} = 0.16$ eV, which is lower than the actual Γ–L valley separation of 0.29 eV. This obvious discrepancy in threshold energy may be attributed once again to thermal smearing effects related to the hot electron distribution in the Γ valley [46], [50], which are not accounted for in our simple model. Table 2 summarizes the best-fit parameters used in the dynamic intervalley-electron-transfer model.

It is well known that a velocity overshoot of electrons can take place under the application of a large DC electric field in GaAs, which is then followed by strong intervalley scattering over sub-picosecond timescales [46]–[48]. For example, the maximum velocity acquired by an electron in GaAs after the application of a DC electric field of 40 kV/cm is about 7×10^7 cm/s [47], [48]. This velocity is reached in a time span of about 150 fs, after which, intervalley scattering to the lower mobility L valley sets in, and the average carrier velocity is greatly reduced. Using the same parameters we used in the dynamic intervalley-electron-transfer model to fit our THz data, a calculation of the average electron velocity $\langle \nu_\Gamma \rangle = (n_\Gamma / n_0)\nu_\Gamma$, upon the application of a step-like 60 kV/cm electric field, revealed a pronounced velocity overshoot in a time less than 200 fs, as shown in Fig. 10. This is consistent with typical velocity overshoot phenomena in GaAs. As such, this provides some justification for the low threshold value for intervalley scattering of $\varepsilon_{th} = 0.16$ eV obtained from our fits, despite the fact that the Γ–L energy separation in GaAs is 0.29 eV. In fact, the energy associated to an electron with a

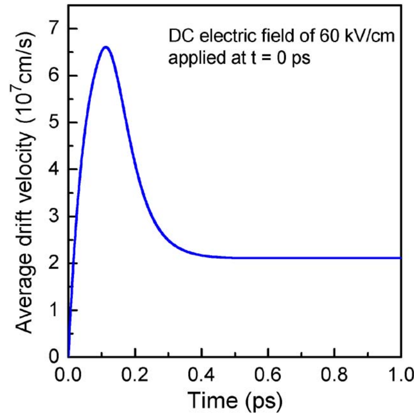

Fig. 10. Time evolution of the average electron drift velocity upon the application of a step-like electric field of 60 kV/cm, according to the dynamic intervalley-electron-transfer model (adapted from [27]).

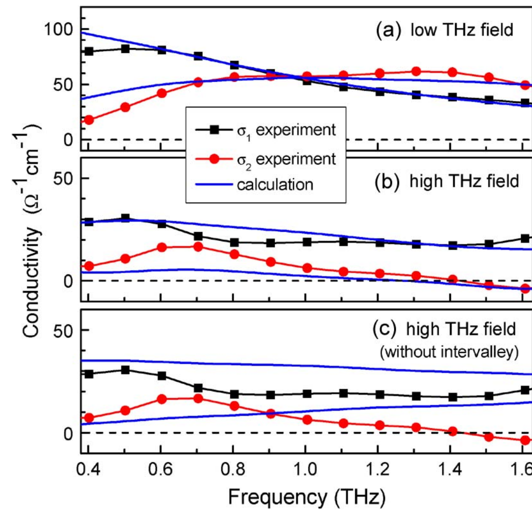

Fig. 11. Real and imaginary part of the complex conductivity extracted at a pump-probe delay time of 10 ps measured at low (a) and high (b) THz probe fields. Blue lines in (a) and (b) are the corresponding fits using the dynamic intervalley-electron-transfer model. (c) The effect of neglecting intervalley scattering in the model (adapted from [27]).

velocity of 7×10^7 cm/s is only 0.1 eV, and yet, this is where intervalley scattering is known to occur in GaAs. We emphasize again that this represents the average electron velocity, and the thermal smearing due to carrier heating effects must be taken into account in a more detailed analysis. Nevertheless, our simple model seems to capture the essential physics of our observations on transient absorption bleaching when we illuminate photoexcited GaAs with intense THz pulses. We note that recent THz-pump/THz-probe measurements have also shown transient absorption bleaching in GaAs due to intervalley scattering [23], [24].

The frequency-dependent complex conductivity $\sigma(\omega)$ in an OPTP experiment can be calculated using [44], [45]:

$$\frac{E_{\text{trans_P}}(\omega)}{E_{\text{trans_R}}(\omega)} = \frac{N+1}{N+1+Z_0 d\sigma(\omega)} \tag{10}$$

where $E_{\text{trans_P}}(\omega)$ and $E_{\text{trans_R}}(\omega)$ are the complex Fourier transforms of the time-domain THz waveforms transmitted through the excited and unexcited GaAs, respectively. Fig. 11 shows the

complex conductivities extracted from the transmitted THz waveforms using (10). At the low THz probe field, the observed conductivity spectrum is consistent with a Drude response [44], [45], [50], as shown in Fig. 11(a). However, the high-field conductivity spectrum shown in Fig. 11(b) differs significantly from the Drude behavior observed at low fields and, in fact, cannot be fitted to any conductivity model. This is simply due to the fact that the conductivity of the photoexcited layer in the GaAs sample is a nonlinear function of the THz probe at high fields. As such, the conductivity cannot be extracted by the simple Fourier analysis used in most OPTP experiments, since this would require the conductivity to be independent from the amplitude of the electric field. This emphasizes once more the need to look at the temporal evolution of the THz waveform rather than the frequency spectrum when probing materials at high peak THz fields. Fig. 11(c) shows how the model fit becomes significantly less accurate if intervalley scattering is ignored.

5. Conclusion

In conclusion, we have performed several nonlinear experiments on the dynamics of free carriers in direct bandgap semiconductors at THz frequencies. Techniques such as Z-scan and OPTP have been employed to explore the nonlinear interactions in both n-doped and photoexcited samples. The mechanism that dominates these kinds of interactions is found to be intervalley scattering and a simple two-valley electron transfer dynamic model coupled with a standard Drude-like response of free carriers in semiconductors well explains the experimental results.

Acknowledgment

The authors are thankful to A. Laramée and F. Poitras for their technical assistance with the ALLS laser source.

References

[1] D. Grischkowsky, S. Keiding, M. van Exter, and C. Fattinger, "Far-infrared time-domain spectroscopy with terahertz beams of dielectrics and semiconductors," *J. Opt. Soc. Amer. B, Opt. Phys.*, vol. 7, no. 10, pp. 2006–2015, Oct. 1990.

[2] D. M. Mittleman, *Sensing With Terahertz Radiation*. Berlin, Germany: Springer-Verlag, 2003.

[3] B. Ferguson and X.-C. Zhang, "Materials for terahertz science and technology," *Nat. Mater.*, vol. 1, no. 1, pp. 26–33, Sep. 2002.

[4] M. R. Leahy-Hoppa, M. J. Fitch, X. Zheng, L. M. Hayden, and R. Osiander, "Wideband terahertz spectroscopy of explosives," *Chem. Phys. Lett.*, vol. 434, no. 4–6, pp. 227–230, Feb. 2007.

[5] S. W. Smye, J. M. Chamberlain, A. J. Fitzgerald, and E. Berry, "The interaction between Terahertz radiation and biological tissue," *Phys. Med. Biol.*, vol. 46, no. 9, pp. R101–R112, Sep. 2001.

[6] S. D. Ganichev and W. Prettl, *Intense Terahertz Excitation of Semiconductors*. Oxford, U.K.: Oxford Univ. Press, 2006.

[7] A. Mayer and F. Keilmann, "Far-infrared nonlinear optics. II. chi (3) contributions from the dynamics of free carriers in semiconductors," *Phys. Rev. B, Condens. Matter*, vol. 33, no. 10, pp. 6962–6968, May 1986.

[8] A. G. Markelz and E. G. Gwinn, "Nonlinear response of quantum-confined electrons in nonparabolic subbands," *J. Appl. Phys.*, vol. 80, no. 4, pp. 2533–2535, Aug. 1996.

[9] A. G. Markelz, N. G. Asmar, B. Brar, and E. G. Gwinn, "Interband impact ionization by terahertz illumination of InAs heterostructures," *Appl. Phys. Lett.*, vol. 69, no. 26, pp. 3975–3977, Dec. 1996.

[10] K. B. Nordstrom, K. Johnsen, S. J. Allen, A. P. Jauho, B. Birnir, J. Kono, T. Noda, H. Akiyama, and H. Sakaki, "Excitonic dynamical Franz–Keldysh effect," *Phys. Rev. Lett.*, vol. 81, no. 2, pp. 457–460, Jul. 1998.

[11] B. E. Cole, J. B. Williams, B. T. King, M. S. Sherwin, and C. R. Stanley, "Coherent manipulation of semiconductor quantum bits with terahertz radiation," *Nature*, vol. 410, no. 6824, pp. 60–63, Mar. 2001.

[12] P. Gaal, K. Reimann, M. Woerner, T. Elsaesser, R. Hey, and K. H. Ploog, "Nonlinear terahertz response of n-type GaAs," *Phys. Rev. Lett.*, vol. 96, no. 18, 187402, May 2006.

[13] Y. Shen, T. Watanabe, D. A. Arena, C. C. Kao, J. B. Murphy, T. Y. Tsang, X. J. Wang, and G. L. Carr, "Nonlinear cross-phase modulation with intense single-cycle terahertz pulses," *Phys. Rev. Lett.*, vol. 99, no. 4, 043901, Jul. 2007.

[14] K. L. Yeh, M. C. Hoffmann, J. Hebling, and K. A. Nelson, "Generation of 10 mJ ultrashort terahertz pulses by optical rectification," *Appl. Phys. Lett.*, vol. 90, no. 17, 171121, Apr. 2007.

[15] F. Blanchard, L. Razzari, H. C. Bandulet, G. Sharma, R. Morandotti, J. C. Kieffer, T. Ozaki, M. Reid, H. F. Tiedje, H. K. Haugen, and F. A. Hegmann, "Generation of 1.5 μJ single-cycle terahertz pulses by optical rectification from a large aperture ZnTe crystal," *Opt. Express*, vol. 15, no. 20, pp. 13212–13220, Oct. 2007.

[16] K.-Y. Kim, J. H. Glownia, A. J. Taylor, and G. Rodriguez, "Terahertz emission from ultrafast ionizing air in symmetry-broken laser fields," *Opt. Express*, vol. 15, no. 8, pp. 4577–4584, Apr. 2007.

[17] J. Hebling, K.-L. Yeh, K. A. Nelson, and M. C. Hoffmann, "High-power THz generation, THz nonlinear optics, and THz nonlinear spectroscopy," *IEEE J. Sel. Topics Quantum Electron.*, vol. 14, no. 2, pp. 345–353, Mar./Apr. 2008.

[18] A. G. Stepanov, L. Bonacina, S. V. Chekalin, and J.-P. Wolf, "Generation of 30 mJ single-cycle terahertz pulses at 100 Hz repetition rate by optical rectification," *Opt. Lett.*, vol. 33, no. 21, pp. 2497–2499, Nov. 2008.
[19] P. Gaal, W. Kuehn, K. Reimann, M. Woerner, T. Elsaesser, R. Hey, J. S. Lee, and U. Schade, "Carrier-wave Rabi flopping on radiatively coupled shallow donor transitions in n-type GaAs," *Phys. Rev. B, Condens. Matter*, vol. 77, no. 23, 235204, Jun. 2008.
[20] Y. Shen, G. L. Carr, J. B. Murphy, T. Y. Tsang, X. Wang, and X. Yang, "Spatiotemporal control of ultrashort laser pulses using intense single-cycle terahertz pulses," *Phys. Rev. A, Gen. Phys.*, vol. 78, no. 4, 043813, Oct. 2008.
[21] H. Wen, M. Wiczer, and A. M. Lindenberg, "Ultrafast electron cascades in semiconductors driven by intense femtosecond terahertz pulses," *Phys. Rev. B, Condens. Matter*, vol. 78, no. 12, 125203, Sep. 2008.
[22] M. C. Hoffmann, J. Hebling, H. Y. Hwang, K.-L. Yeh, and K. A. Nelson, "Impact ionization in InSb probed by terahertz pump–terahertz probe spectroscopy," *Phys. Rev. B, Condens. Matter*, vol. 79, no. 16, 161201, Apr. 2009.
[23] M. C. Hoffmann, J. Hebling, H. Y. Hwang, K.-L. Yeh, and K. A. Nelson, "THz-pump/THz-probe spectroscopy of semiconductors at high field strengths [Invited]," *J. Opt. Soc. Amer. B, Opt. Phys.*, vol. 26, no. 9, pp. A29–A34, Sep. 2009.
[24] J. Hebling, M. C. Hoffmann, H. Y. Hwang, K.-L. Yeh, and K. A. Nelson, "Observation of nonequilibrium carrier distribution in Ge, Si, and GaAs by terahertz pump–terahertz probe measurements," *Phys. Rev. B, Condens. Matter*, vol. 81, no. 3, 035201, Jan. 2010.
[25] M. C. Hoffmann, N. C. Brandt, H. Y. Hwang, K.-L. Yeh, and K. A. Nelson, "Terahertz Kerr effect," *Appl. Phys. Lett.*, vol. 95, no. 23, 231105, Dec. 2009.
[26] L. Razzari, F. H. Su, G. Sharma, F. Blanchard, A. Ayesheshim, H. C. Bandulet, R. Morandotti, J. C. Kieffer, T. Ozaki, M. Reid, and F. A. Hegmann, "Nonlinear ultrafast modulation of the optical absorption of intense few-cycle terahertz pulses in n-doped semiconductors," *Phys. Rev. B, Condens. Matter*, vol. 79, no. 19, 193204, May 2009.
[27] F. H. Su, F. Blanchard, G. Sharma, L. Razzari, A. Ayesheshim, T. L. Cocker, L. V. Titova, T. Ozaki, J. C. Kieffer, R. Morandotti, M. Reid, and F. A. Hegmann, "Terahertz pulse induced intervalley scattering in photoexcited GaAs," *Opt. Express*, vol. 17, no. 12, pp. 9620–9629, Jun. 2009.
[28] A. Rice, Y. Jin, X. F. Ma, X. C. Zhang, D. Bliss, J. Larkin, and M. Alexander, "Terahertz optical rectification from $\langle 110 \rangle$ zinc-blende crystals," *Appl. Phys. Lett.*, vol. 64, no. 11, pp. 1324–1326, Mar. 1994.
[29] Q. Wu and X. C. Zhang, "Ultrafast electro-optic field sensors," *Appl. Phys. Lett.*, vol. 68, no. 12, pp. 1604–1606, Mar. 1996.
[30] P. C. M. Planken, H.-K. Nienhuys, H. J. Bakker, and T. Wenckebach, "Measurement and calculation of the orientation dependence of terahertz pulse detection in ZnTe," *J. Opt. Soc. Amer. B, Opt. Phys.*, vol. 18, no. 3, pp. 313–317, Mar. 2001.
[31] M. Sheik-Bahae, A. A. Said, T. H. Wei, D. J. Hagan, and E. W. Van Stryland, "Sensitive measurement of optical nonlinearities using a single beam," *IEEE J. Quantum Electron.*, vol. 26, no. 4, pp. 760–769, Apr. 1990.
[32] B. Gu, W. Ji, P. S. Patil, S. M. Dharmaprakash, and H.-T. Wang, "Two-photon-induced excited-state absorption: Theory and experiment," *Appl. Phys. Lett.*, vol. 92, no. 9, 091118, Mar. 2008.
[33] A. D. Lad, P. P. Kiran, G. R. Kumar, and S. Mahamuni, "Three-photon absorption in ZnSe and ZnSe/ZnS quantum dots," *Appl. Phys. Lett.*, vol. 90, no. 13, 133113, Mar. 2007.
[34] S. E. Ralph, Y. Chen, J. Woodall, and D. McInturff, "Subpicosecond photoconductivity of $In_{0.53}Ga_{0.47}As$: Intervalley scattering rates observed via THz spectroscopy," *Phys. Rev. B, Condens. Matter*, vol. 54, no. 8, pp. 5568–5573, Aug. 1996.
[35] M. C. Nuss and J. Orenstein, "THz time domain spectroscopy," in *Millimeter and Submillimeter Wave Spectroscopy of Solids*. Berlin, Germany: Springer-Verlag, 1998.
[36] K. Blotekjaer, "Transport equations for electrons in two-valley semiconductors," *IEEE Trans. Electron Devices*, vol. ED-17, no. 1, pp. 38–47, Jan. 1970.
[37] A. M. Anile and S. D. Hern, "Two-valley hydrodynamical models for electron transport in gallium arsenide: Simulation of Gunn oscillations," *VLSI Des.*, vol. 15, no. 4, pp. 681–693, Jan. 2002.
[38] J. Singh, *Electronic and Optoelectronic Properties of Semiconductor Structures*. Cambridge, U.K.: Cambridge Univ. Press, 2003.
[39] M. A. Haase, V. M. Robbins, N. Tabatabaie, and G. E. Stillman, "Subthreshold electron velocity-field characteristics of GaAs and $In_{0.53}Ga_{0.47}As$," *J. Appl. Phys.*, vol. 57, no. 6, pp. 2295–2298, Mar. 1985.
[40] S. R. Ahmed, B. R. Nag, and M. D. Roy, "Hot-electron transport in $In_{0.53}Ga_{0.47}As$," *Solid-State Electron.*, vol. 28, no. 12, pp. 1193–1197, Dec. 1985.
[41] S. Adachi, "Model dielectric constants of GaP, GaAs, GaSb, InP, InAs, and InSb," *Phys. Rev. B, Condens. Matter*, vol. 35, no. 14, pp. 7454–7463, May 1987.
[42] P. C. Becker, H. L. Fragnito, C. H. B. Cruz, J. Shah, R. L. Fork, J. E. Cunningham, J. E. Henry, and C. V. Shank, "Femtosecond intervalley scattering in GaAs," *Appl. Phys. Lett.*, vol. 53, no. 21, pp. 2089–2090, Nov. 1988.
[43] A. Ghosal, D. Chattopadhyay, and N. N. Purkait, "Hot-electron velocity overshoot in $Ga_{0.47}In_{0.53}As$," *Appl. Phys. Lett.*, vol. 44, no. 8, pp. 773–774, Apr. 1984.
[44] R. P. Prasankumar, A. Scopatz, D. J. Hilton, A. J. Taylor, R. D. Averitt, J. M. Zide, and A. C. Gossard, "Carrier dynamics in self-assembled ErAs nanoislands embedded in GaAs measured by optical-pump terahertz-probe spectroscopy," *Appl. Phys. Lett.*, vol. 86, no. 20, 201107, May 2005.
[45] D. G. Cooke, F. A. Hegmann, E. C. Young, and T. Tiedje, "Electron mobility in dilute GaAs bismide and nitride alloys measured by time-resolved terahertz spectroscopy," *Appl. Phys. Lett.*, vol. 89, no. 12, 122103, Sep. 2006.
[46] M. Lundstrom, *Fundamentals of Carrier Transport*. Cambridge, U.K.: Cambridge Univ. Press, 2000.
[47] M. Grundmann, *The Physics of Semiconductors*. Berlin, Germany: Springer-Verlag, 2006.
[48] B. E. Foutz, S. K. O'Leary, M. S. Shur, and L. F. Eastman, "Transient electron transport in wurtzite GaN, InN, and AlN," *J. Appl. Phys.*, vol. 85, no. 11, pp. 7727–7734, Jun. 1999.
[49] M. C. Nuss, D. H. Auston, and F. Capasso, "Direct subpicosecond measurement of carrier mobility of photoexcited electrons in gallium arsenide," *Phys. Rev. Lett.*, vol. 58, no. 22, pp. 2355–2358, Jun. 1987.

[50] M. C. Beard, G. M. Turner, and C. A. Schmuttenmaer, "Transient photoconductivity in GaAs as measured by time-resolved terahertz spectroscopy," *Phys. Rev. B, Condens. Matter*, vol. 62, no. 23, pp. 15 764–15 777, Dec. 2000.
[51] P. N. Saeta, J. F. Federici, B. I. Greene, and D. R. Dykaar, "Intervalley scattering in GaAs and InP probed by pulsed far-infrared transmission spectroscopy," *Appl. Phys. Lett.*, vol. 60, no. 12, pp. 1477–1479, Mar. 1992.
[52] Q.-L. Zhou, Y. Shi, B. Jin, and C. Zhang, "Ultrafast carrier dynamics and terahertz conductivity of photoexcited GaAs under electric field," *Appl. Phys. Lett.*, vol. 93, no. 10, 102103, Sep. 2008.